Tuning the Chemical Environment within the UiO-66-NH2 Nanocages for Charge-Dependent Contaminant Uptake and Selectivity

Ibrahim, Ahmed H.; El-Mehalmey, Worood A.; Haikal, Rana R.; Safy, Mohamed E. A.; Amin, Muhamed; Shatla, Hassan R.; Karakalos, Stavros G.; Alkordi, Mohamed H.

Published in:
Inorganic Chemistry

DOI:
10.1021/acs.inorgchem.9b01611

Publication date:
2019

Inorganic Chemistry
Article
Cite This: Inorg. Chem. XXXX, XXX, XXX−XXX
pubs.acs.org/IC

Tuning the Chemical Environment within the UiO-66-NH_2 Nanocages for Charge-Dependent Contaminant Uptake and Selectivity

Ahmed H. Ibrahim,[†,∥] Worood A. El-Mehalmey,[†,∥] Rana R. Haikal,[†] Mohamed E. A. Safy,[†] Muhamed Amin,[‡] Hassan R. Shatla,[†] Stavros G. Karakalos,[§] and Mohamed H. Alkordi*[,†]

[†]Center for Materials Science, Zewail City of Science and Technology, October Gardens, Giza 12578, Egypt
[‡]Department of Sciences, University College Groningen, University of Groningen, 9718 BG Groningen, Netherlands
[§]College of Engineering and Computing, Swearingen Engineering Center, University of South Carolina, Columbia, South Carolina 29208, United States

Supporting Information

ABSTRACT: The remarkable water stability of Zr-carboxylate-based metal−organic frameworks (MOFs) stimulated considerable interest toward their utilization in aqueous phase applications. The origin of such stability is probed here through pH titration and pK_a modeling. A unique feature of the $Zr_6(\mu_3\text{-}OH)_4(\mu_3\text{-}O)_4(RCO_2)_{12}$ cluster is the Zr-bridging oxo/hydroxyl groups, demonstrating several pK_a values that appear to provide for the water stability at a wide range of pH. Accordingly, the tunability of the cage/surface charge of the MOF can feasibly be controlled through careful adjustment of solution pH. Such high stability, and facile control over cage/surface charge, can additionally be augmented through introducing chemical functionalities lining the cages of the MOF, specifically amine groups in the UiO-66-NH_2 presented herein. The variable protonation states of the Zr cluster and the pendant amino groups, their H-bond donor/acceptor characteristics, and their electrostatic interactions with guest molecules were effectively utilized in controlled experiments to demonstrate high uptake of model guest molecules (137 mg/g for Cr(VI), 1275 mg/g for methylene blue, and 909 mg/g for methyl orange). Additionally, a practical form of the silica-supported MOF, UiO-66-NH_2@SiO_2, constructed in under 2 h reaction time, is described, generating a true platform microporous sorbent for practical use in demanding applications.

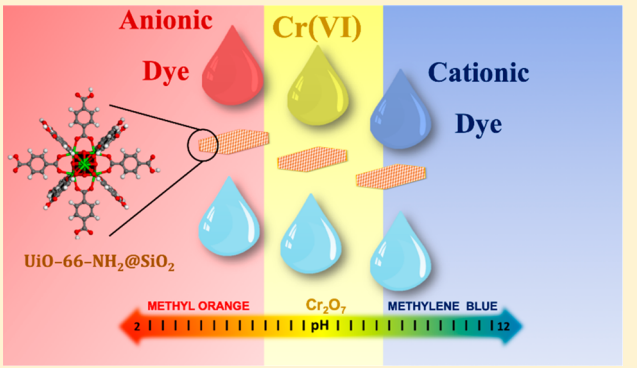

INTRODUCTION

The large family of microporous solids, commonly known as metal−organic frameworks (MOFs), has attracted significant interest in the past two decades due to the demonstrated designer synthesis approach allowing reticular synthesis of functional solids.[1] Through judicious choice of molecular building units (MBUs), fine-tuning of MOFs' composition and structure is readily attainable.[2] Such structure/function malleability opened a potentially unlimited chemical space for generating a plethora of microporous solids with far reaching applications. MOFs continue to demonstrate outstanding performance in a wide range of applications including gas sorption and separation,[3−7] heterogeneous catalysis,[8−12] as well as energy storage applications.[13−17]

Despite the common instability of a large number of MOFs in aqueous media, the Zr-carboxylate MOF (UiO-66) demonstrates an impressive aqueous stability under a wide range of pH.[18] Properly functionalized derivatives of the Zr-MOF (e.g., the UiO-66-NH_2) therefore hold potential for water-based applications.[19−22]

Despite a relatively large number of reports on the removal of organic dyes from water, the interest in probing MOFs utilization for Cr(VI) removal is rapidly growing.[23−27] Furthermore, the utilization of a single MOF, as a platform material, is yet to be demonstrated in real-life wastewater treatment. Herein, we outline several factors necessary to include in novel platform sorbents for wastewater treatment including (1) chemical stability at a wide range of pH, (2) tunability toward optimal/selective uptake of contaminants, (3) demonstrated regeneration and recyclability, and (4) amenability to formulation allowing ease of recoverability/separation from the treated solution. Herein, an optimized synthesis of the UiO-66-NH_2 on silica microparticles (UiO-66-NH_2@SiO_2)[30,31] is demonstrated, surmounting the difficult retrieval of the nanocrystalline UiO-66-NH_2 MOF (*ca.* 50−150 nm)[28] from solution. This much-improved synthesis effectively limits the time for constructing the MOF@SiO_2

Received: May 31, 2019

DOI: 10.1021/acs.inorgchem.9b01611
Inorg. Chem. XXXX, XXX, XXX−XXX

composite to only 2 h, and at a mild 80 °C. Additionally, the chemical changes induced in the nanocages of the MOF and on the surface of its crystals at a wide range of solution pH were experimentally investigated and computationally simulated. Such changes were found to result in tunable sorption capability of the same platform UiO-66-NH_2@SiO_2 material toward different guest molecules: dichromate ions, methylene blue, and methyl orange.

RESULTS AND DISCUSSION

The synthesis of the UiO-66-NH_2@SiO_2 proceeded successfully by inclusion of the suspended silica gel microparticles (100−160 μm) in the reaction mixture containing $ZrCl_4$ and the organic ligand. Key to isolating silica microparticles homogeneously coated by a crust of the UiO-66-NH_2 nanocrystals was the constant stirring of the synthesis mixture to ensure homogeneous nucleation/growth of the MOF nanocrystals on the silica particles, Scheme 1. The addition

Scheme 1. Synthesis of the Surface-Anchored UiO-66-NH_2@SiO_2

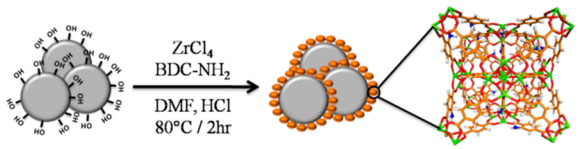

of HCl to the reaction mixture was shown previously to greatly facilitate the reaction,[28] where in this setup it was sufficient to maintain the mixture at 80 °C for only 2 h to isolate the UiO-66-NH_2@SiO_2. It is assumed that the surface hydroxyl groups of the silica particles acted as anchoring sites to immobilize Zr(IV) ions, upon which subsequent coordination by the ligand molecules initiated the formation of the MOFs nanocrystals (133−178 nm) on the surface of the silica particles. The scanning electron microscopy (SEM) images, Figure 1, clearly demonstrate the continuous and homogeneous coating of the silica microparticles with the MOF nanocrystals. When compared to the SEM of the silica particles, Figure S1, the continuous and homogeneous deposition of the MOF nanocrystallites on the silica surface becomes evident. This UiO-66-NH_2@SiO_2 form facilitated the subsequent investigations, overcoming the challenge of forming fine suspension of the MOF nanocrystals in the test media.

Further confirmation for the formation of the targeted MOF on the surface of the SiO_2 microparticles was obtained from the X-ray diffraction pattern (XRD) recorded for the UiO-66-NH_2@SiO_2 as compared to the pattern calculated for the UiO-66, Figure 2. It is evident that all characteristic peaks of the UiO-66-NH_2 were observed in the UiO-66-NH_2@SiO_2, with no distinctive peaks for the amorphous silica support. Additionally, the FTIR spectrum of the UiO-66-NH_2@SiO_2 demonstrated combined features of its two components, Figures S2 and S3 in the Supporting Information (SI). The characteristic peaks for the MOF included the C═O str. for the carboxylate at 1652 cm^{-1}, the C═C str. at 1568 cm^{-1}, as well as the characteristic Si−O str. at 1058 cm^{-1} and the O−H band at 3250 cm^{-1}. The UiO-66-NH_2@SiO_2 was found to be microporous with a calculated BET surface area of 630 m^2/g, Figure S4. The synthesis condition utilized here is sufficiently acidic, inducing formation of the protonated ammonium

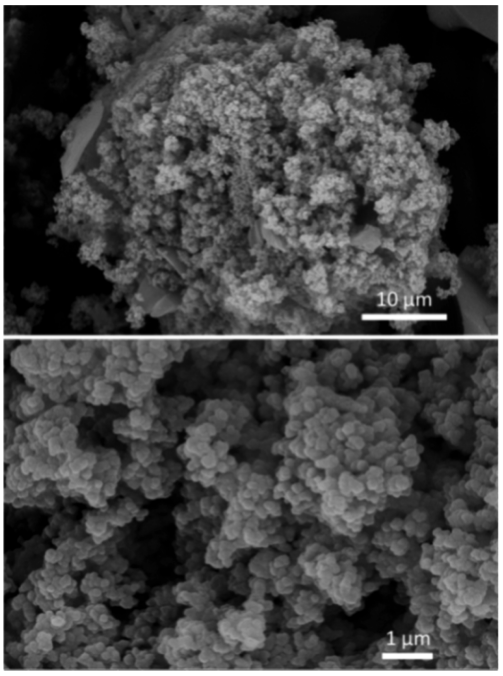

Figure 1. SEM images of the UiO-66-NH_2@SiO_2 at two different magnifications, showing complete and homogeneous coating of the SiO_2microparticle (top) by the MOF nanocrystals and (below) the topography of the MOF crust.

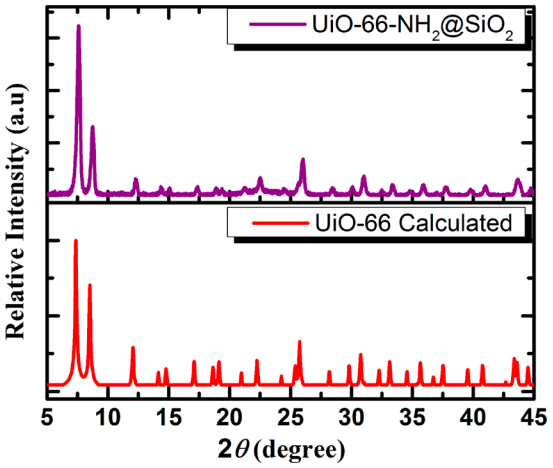

Figure 2. XRD pattern for the UiO-66-NH_2@SiO_2 compared to the calculated pattern for UiO-66, confirming the formation of the MOF atop the silica microparticles.

conjugate acid of the MOF, as well as inducing missing node defects.[29] The chemical environment at the aromatic amine was probed by X-ray photoelectron spectroscopy (XPS), Figure 3. The N 1s peak recorded for the MOF before and after uptake of dichromate ions indicated the presence of $-NH_2$ as well as $-NH_2/NH_3^+$ (H-bonded/ammonium species). The BE of 399.3 eV for the N 1s is typically associated with $-NH_2$ species, while the BE in the range of 400 eV is characteristic of H-bonded and/or quaternary ammonium species.[30] The deconvoluted N 1s lines, Figure 3b, clearly demonstrated an enhanced component at higher BE for the Cr-treated sample, indicating H-bond interactions within the nanocages. The O 1s spectrum for the as-synthesized MOF showed a characteristic B.E at 533 eV, which can be assigned

DOI: 10.1021/acs.inorgchem.9b01611
Inorg. Chem. XXXX, XXX, XXX−XXX

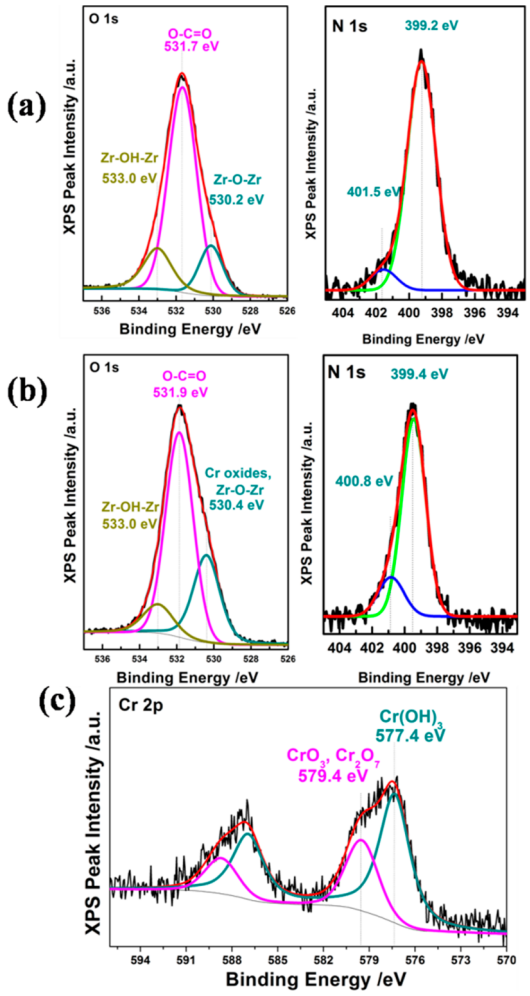

Figure 3. XPS spectra for (a) the UiO-66-NH_2 and (b,c) the UiO-66-NH_2 after dichromate uptake by the MOF.

to a bridging hydroxyl (μ_3-OH), 531.7 eV ascribed to Zr-carboxylate, and 530.2 eV assigned to (μ_3-O) in Zr−O−Zr.[31] After adsorption of dichromate, an increase in relative intensity of the peak at 530.4 eV and a decrease in the relative intensity of the 533 eV peak can thus be ascribed to adsorbed dichromate ions. The microanalysis atomic % values recorded on samples of the MOF before and after treatment with dichromate ions are provided in Table 1. It is noticeable that

Table 1. XPS Analysis Showing Atomic % for the Several Elements in the As-Synthesized MOF and That after Impregnation with Cr(VI) through Soaking in 100 ppm of $Cr_2O_7^{2-}$ Solution

element (atomic %)	Zr	C	N	Cl	O	Cr
MOF	5.7	55.7	5.9	2.6	30.1	0
Cr@MOF	6.0	52.0	5.6	1.4	32.9	2.1

the as-synthesized MOF contained appreciable amounts of Cl ions, most probably present as counterions to ammonium species. It is interesting to notice that the Cl atomic % is half that of the N, indicating that protonation occurred only to half the present amine groups under the synthesis conditions. This assignment was further supported by experimental observation showing enhanced dichromate uptake upon first washing the MOF with 0.1 M HCl solution to further protonate pendant amine groups, thus enhancing the H-bond interactions with dichromate ions. After treatment with dichromate solution, a noticeable decrease of the Cl atom % indicated that dichromate was adsorbed within the MOF cages through the ion-exchange process, displacing the chloride counterions. The observation of Cr(III) in the XPS is notable, which could indicate the occurrence of redox interactions. However, it is more likely that these Cr(III) ions resulted from *in situ* reduction of the highly electronegative dichromate ion under the high energy radiation utilized in XPS.[32,33] The possibility of redox interactions with the MOF can safely be ruled out based on observed high recyclability/regeneration of the MOF for at least 10 cycles without losing its activity (recyclability test *vide infra*). In order to further probe the microenvironment within the nanocages of the MOF, a pH dependence uptake investigation was conducted utilizing two deliberately selected molecular probes, methyl orange (MO) and methylene blue (MB). The two molecules were selected in anticipation of the chemical nature of the probe, the microporous host, and structural variation that can occur in both the host and the guest molecules according to the pH of the solution. This investigation was facilitated by demonstrated notable stability of the UiO-66-NH_2 under a wide range of pH.[18,34] The anionic MO molecule contains the sulfonic acid group, capable of H-bond interactions with the (μ_3-OH) and amino/ammonium groups decorating the cages of the MOF. On the other hand, the MB molecule is cationic and lacking strong H-bond moieties. The observed trend of dye uptake by the MOF@SiO_2 (reported as milligrams of dye adsorbed per gram of MOF@SiO_2) in relation to the pH of the solution is shown in Figure 4. It is evident that at acidic pH, where the

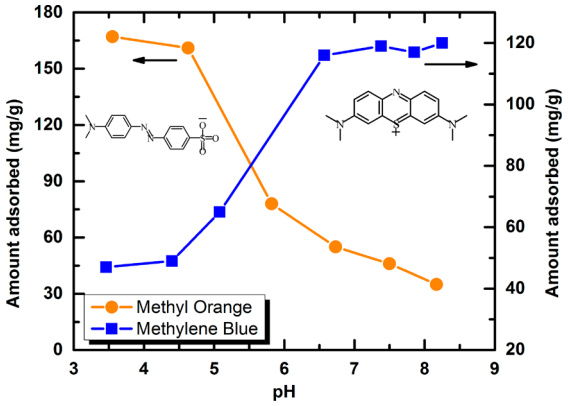

Figure 4. Uptake dependence on solution pH for MB and MO (initial concentration 160 ppm for MO and 121 ppm for MB) adsorbed within the UiO-66-NH_2@SiO_2.

protonated form of the UiO-66-NH_2 is dominant, the MOF adsorbed the anionic, H-bond acceptor MO molecules much more preferentially than MB. A striking flip of the sorbent capability, reflecting change in the cage protonation state, was observed beyond pH ~ 5.6. At higher pH values than 5.6, the MOF did not demonstrate appreciable uptake of the anionic MO molecules, reflecting preferred solvation of the molecules over adsorption within the host. On the contrary, the MOF@SiO_2 at pH values higher than 5.6 demonstrated increasing capacity of the cationic MB molecular probe. To further demonstrate the tunable selectivity of the MOF toward specific guest, triggered by solution pH, a mixture of MO and MB was utilized for adsorption into UiO-66-NH_2@SiO_2. As shown in

DOI: 10.1021/acs.inorgchem.9b01611
Inorg. Chem. XXXX, XXX, XXX−XXX

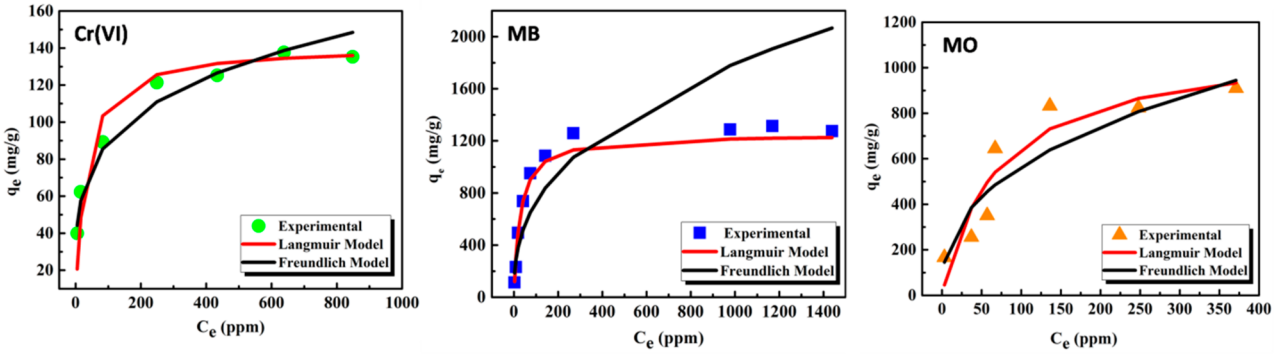

Figure 5. Adsorption isotherms for Cr(VI) at pH = 5.4, MB at pH = 9.7, and MO at pH = 3.5 on the UiO-66-NH_2@SiO_2.

Figure S5, when the mixture was maintained at acidic pH, the selective uptake of MO was noticed, while when the pH was raised to 9.5, selective uptake of the MB was recorded from the mixture. This experiment clearly demonstrated the tunable cage chemistry simply by controlling the pH of the solution, triggering selective guest uptake by the MOF. A similar trend was also observed for the MOF powder in the absence of silica, see Figure S6, confirming the observed behavior to originate from the MOF cages. Interestingly, the uptake capacity of the MOF@SiO_2 toward MO and MB was almost equal at pH 5.6. As this pH is the isoelectric point of the MOF@SiO_2 (evident from the zeta potential measurements, *vide infra*), this observation indicated that, at solution pH matching the isoelectric point of the MOF, simple molecular diffusion and adsorption is operative. Maintaining the MOF@SiO_2 at a solution of pH 5.6 thus resulted in shutting down the charge-assisted uptake mechanism for the cages, resulting in almost equal and nonpreferential uptake of the guest molecules. To assess the maximum uptake capacity of the UiO-66-NH_2@SiO_2 toward Cr(VI), MO, and MB, the corresponding adsorption isotherms were constructed at the optimal pH value, Figure 5 (see Figures S7–S11 for further details). For each sorbate, the optimal pH of the solution was adjusted to 5.4 Cr(VI), 3.5 (MO), and 9.7 (MB) based on the observed trend from the pH dependent uptake study. The UiO-66-NH_2@SiO_2 demonstrated exceptionally high uptake (137 mg/g for Cr(VI), 1275 mg/g for MB, and 909 mg/g for MO). To ascertain the observed capacities originating from adsorption within the MOF cages, similar trials were conducted on the MOF powder (no silica included) where it demonstrated an adsorption capacity of 1202 mg/g for MB and 859 mg/g for MO. In the three investigated adsorbates, the experimental data can be more closely fitted with the Langmuir model, Table 2, indicating strong sorbent–sorbate interactions leading to monolayer adsorption within the MOF. Although several reports demonstrated the high uptake of MOFs,[45] it is noteworthy that, to the best our knowledge, such high uptake of MO and MB was not recorded in the UiO-66-NH_2 previously. Table 3 lists the reported removal capacities for MO and MB by MOF adsorbents, including UiO-66/-NH_2. It is also worth mentioning that the simultaneous uptake of both cationic and anionic dyes, represented herein by MB and MO, respectively, has not been reported with such high capacities using the same adsorbent. This is attributed to the optimized conditions utilized here for the preferential uptake of either MB or MO by the MOF. In an attempt to further investigate the charge state of the UiO-66-NH_2 particles, zeta potential measurements across a wide pH range were conducted, Figure 6. The MOF crystals demonstrated positive zeta potential in the acidic pH range, flipping to negative zeta potential at values higher than pH 5.6. This further confirms the proposed model of protonated MOF cages at acidic pH and the formation of neutral to negatively charged particles in neutral/basic pH. This behavior can be ascribed to hydroxyl ion adsorption/coordination, as well as deprotonation of pendant ammonium groups. In a recent study, upon increasing the amount of acid added to the synthesis of UiO-66-NH_2, a corresponding increase of zeta potential was observed.[46,48] The UiO-66

Table 2. Adsorption Isotherms Parameters for Uptake of the Three Adsorbates within UiO-66-NH_2@SiO_2

	Langmuir			Freundlich		
adsorbate	q_m	b	R^2	K_f	n	R^2
Cr(VI)	141	0.033	0.997	29.92	4.21	0.973
MO	1111	0.014	0.921	94.47	2.57	0.847
MB	1250	0.035	0.999	121.42	2.57	0.839

Table 3. Dye Removal Capacities for Several MOFs from Aqueous Solution

	dye removal capacity (mg/g)		
material	MO	MB	ref
MOF-235	477	187	35
MIL-68(Al)	341.3		36
Cu-BDC	86.71		37
$H_6P_2Mo_{15}W_3O_{62}$/MOF-5		401.6	38
GO/MOF		274	39
Cd(II)Organic Framework		149	40
Fe_3O_4@NH_2-MIL-101(Cr)		370.3	41
MFC-N-100		358	42
NH_2-MIL-125		405.61	43
MIL-125		321.39	
UiO-66		91	44
UiO-66		107	45
UiO-66[a]	84.8	13.2	46
UiO-66	28.97	96.45	47
UiO-66-NH_2	39.4	90.88	
UiO-66-NH_2@SiO_2[b]	909	1275	this work

[a]Acetic acid was used as modulator during MOF synthesis. [b]The values represent adsorption within the MOF; contribution from silica as sorbent in control experiments is accounted for (see experimental section).

DOI: 10.1021/acs.inorgchem.9b01611
Inorg. Chem. XXXX, XXX, XXX–XXX

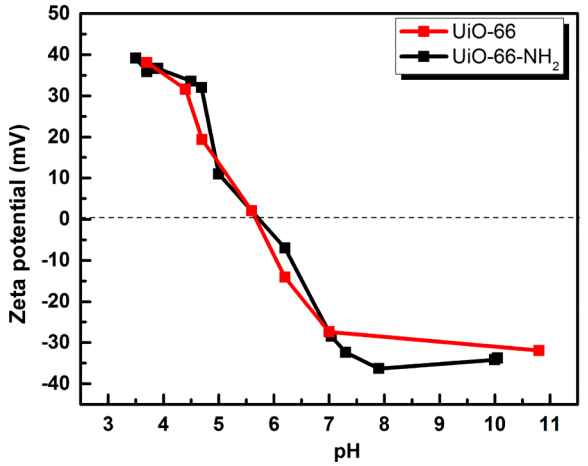

Figure 6. Zeta potential measurements for UiO-66 and UiO-66-NH_2 at different pH values.

crystals also demonstrated similar zeta potential behavior at the investigated solution pH, indicating that the surface charge in the UiO-66/-NH_2 family originates mainly from variable protonation stages of the Zr cluster.

It was shown recently that the (μ_3-OH) groups within the Zr clusters of the UiO-66 possess acidic character with pK_a = 3.52.[49] Furthermore, the same study indicated that missing linkers from the solid caused by the addition of an acid modulator during the synthesis can be substituted by Zr-coordinated water and hydroxyls, thus furnishing two potential ionizable protons with calculated pK_a values of 6.79 and 8.30, respectively.[49] However, a similar experimental investigation was not conducted on the UiO-66-NH_2. We have therefore conducted its potentiometric titration, Figure 7, which clearly

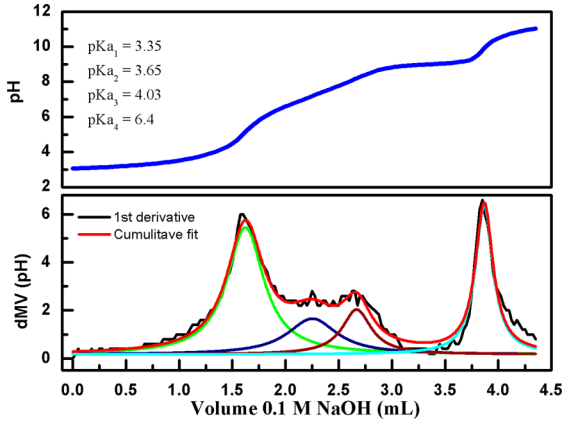

Figure 7. Potentiometric titration of UiO-66-NH_2 in aqueous solution (top), showing the first derivative and the corresponding deconvolution pattern (bottom).

indicates a noticeable difference from that previously reported for UiO-66. We speculate that the Zr cluster acts as a weak polyprotic acid through its bridging hydroxyl ions. In the conducted titration, four discernible pK_a values for the UiO-66-NH_2 were recorded, Figure 7. The observed pK_a values (3.35, 3.65, 4.03, 6.4) can tentatively be ascribed to the pendant ammonium groups and the bridging hydroxyl (μ_3-OH) groups within the Zr clusters, where we hypothesize that such groups do not have equivalent pK_a values, due to efficient electronic coupling, rendering progressive deprotonation on the same cluster less spontaneous. The first observed pK_a (3.35) can thus be ascribed to the deprotonation of the first (μ_3-OH), which is comparable to that previously reported for UiO-66.[49] The second observed pK_a (3.65) is most likely due to the deprotonation of the pendant ammonium groups.[50] The two succeeding pK_a values (4.03 and 6.4) can thus be assigned to further (μ_3-OH) groups within the Zr clusters. The vast difference between the late pK_a values can be ascribed to less favored ionization of the μ_3-OH due to buildup of negative charge on the Zr cluster. To test this hypothesis, the pK_a values for all the bridging oxygen atoms (in oxide and hydroxide bridging ions) in a model Zr-acetate cluster were calculated, see Figure 8 and the Experimental Methods. The calculated

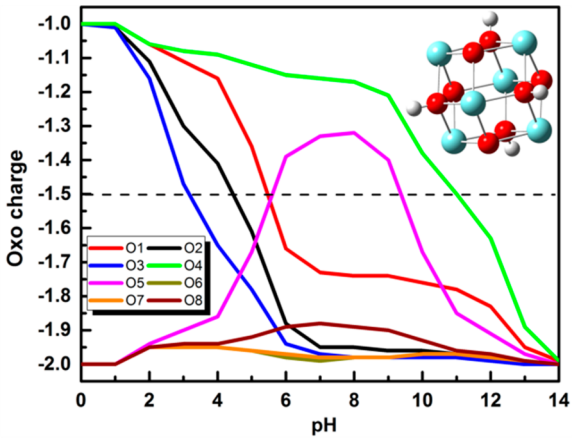

Figure 8. Calculated titration curve for the eight oxygen atoms in the cluster $[Zr_6(OH)_4(O)_4(CH_3CO_2)_{12}]$ indicating successive deprotonation stages for the μ_3-OH groups. O1−O4 represent μ_3-OH; O5−O8 represent μ_3-O.

pK_a values for the μ_3-OH groups were taken to be the pH values at which bridging oxo groups have a calculated formal charge of −1.5, indicating the protonation state between hydroxide and oxide species. The calculated pK_a values were found to be 3.15, 4.43, 6.9, and 11. The two intersecting lines for O1 and O5 ions in Figure 8 indicate back-titration behavior where the two O sites demonstrate prototropic tautomerization. The calculations clearly demonstrated four discernible pK_a values for the μ_3-OH groups, reflecting strong electronic/electrostatic interactions between the Zr-bridged oxide/hydroxide groups.

The good correlation observed here between the experimentally measured pK_a values and those calculated was only established for the first three deprotonation steps. The high pK_a value for the last deprotonation step was not captured by the experiment due to instability of the MOF at pH values higher than 11. The calculations also revealed fairly low pK_a values for the bridging oxide species, indicating that under the normal working conditions of the UiO-66-NH_2, the bridging oxide groups are in their conjugate base (oxide) form.

It is known that missing linker structural defects can occur at the Zr-carboxylate clusters in UiO-66 MOF, where a currently proposed model describes Zr-bound water molecules replacing the missing linker Zr−O bond, albeit with a hydroxide ion at H-bonding distance to one of the bridging hydroxyl ions, balancing the charge of the cluster.[51] This type of defective cluster can thus be regarded as cationic under slightly acidic conditions where solution pH limits the concentration of free

DOI: 10.1021/acs.inorgchem.9b01611
Inorg. Chem. XXXX, XXX, XXX−XXX

hydroxyl ions. The observed change in zeta potential for the MOF crystallites, taking place around pH = 5.6, is therefore in agreement with this proposed model. Although the pK_a model presented here is for the nondefective cluster, nonetheless, the results discussed here reflect the rich chemistry of the Zr-carboxylate cluster and hints into the origin of the observed high stability of the UiO-66 MOF family at a wide range of solution pH. It is proposed here that the Zr-carboxylate cluster has variable degrees of protonation for the Zr-bridging (μ_3-OH) ions, thus protecting the cluster from nucleophilic attack by solvated hydroxide ions. The observed pH dependence of the cage chemistry and accordingly the surface charge of the MOF have thus resulted in modulating its ability to preferentially uptake the studied guest molecules. Whereupon, under sufficiently acidic conditions, the positively charged cages facilitated uptake of the MO and dichromate ions, while at neutral to basic solution, MB was preferentially adsorbed by the negatively charged cages of the MOF.

To investigate the role of the amine functionality in enhancing the uptake capacity toward the different guest molecules, the UiO-66@SiO_2 was synthesized under essentially similar conditions to those used here for the amine counterpart and tested for uptake of the three contaminants. As the UiO-66@SiO_2 demonstrated lower capacities as compared to the amine derivative, Figure 9, the relative

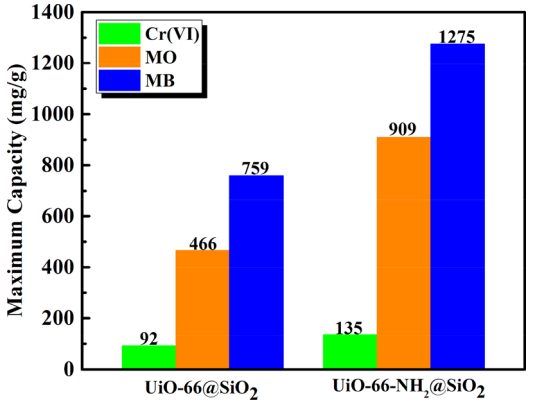

Figure 9. Comparison of maximum adsorption capacity between UiO-66@SiO_2 and UiO-66-NH_2@SiO_2 for Cr(VI), MO, and MB.

significance of the two binding sites can be discernible. The higher uptake observed for the UiO-66-NH_2@SiO_2 can rationally be ascribed to further (H-bond) interactions with the amine/ammonium groups within the cages of the MOF. It is therefore suggested that uptake of specific adsorbates by the UiO-66-NH_2@SiO_2 is facilitated by (a) the surface charge of the crystals, controllable through the pH of the synthesis mixture and the sorption medium, (b) the ability to alter the charge on the Zr nodes by controlling the solution pH, and (c) the presence of amine/ammonium groups capable of charge-assisted H-bond interactions with the guest molecules.

The recyclability of the solid sorbent toward the three investigated sorbates was then examined. Utilizing a syringe filter setup, passing a solution of the three different sorbates through the UiO-66-NH_2@SiO_2 and measurement of the residual concentration of the contaminant up to 10 cycles is demonstrated in Figure 10. After each passage, the material was regenerated as described in the Experimental Methods, and the recyclability was demonstrated in the three cases, most notable in the case of MO. It is thus demonstrated that this

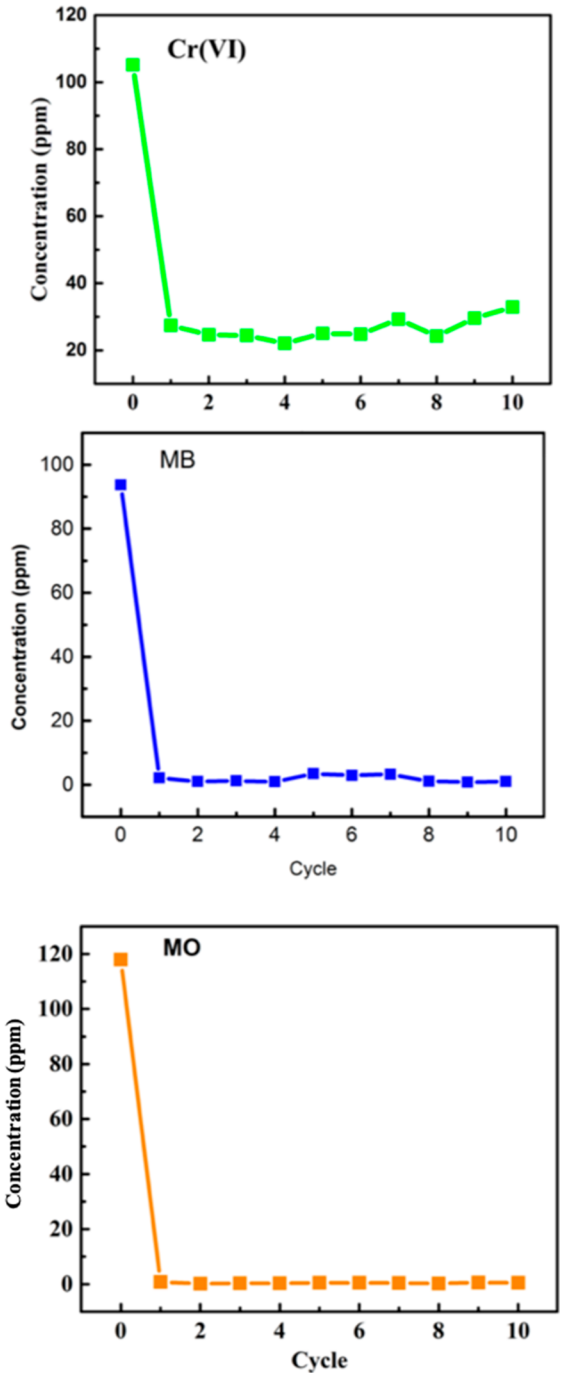

Figure 10. Recyclability test for removal of Cr(VI), MB, and MO on the UiO-66-NH_2@SiO_2.

system is truly a platform microporous sorbent for facile, rapid, and controllable removal of model contaminants with a diverse chemical nature, all facilitated through the efficient formulation and the malleable cage chemistry of the sorbent.

CONCLUSION

In this study, we present a practical and easy-to-use form of UiO-66-NH_2@SiO_2, constructed in a 2 h reaction time, overcoming the limitation of fine particle size for practical end applications. Furthermore, the MOF@SiO_2 was found to demonstrate high uptake capacity for dichromate ions from aqueous solution, with high stability and recyclability for

DOI: 10.1021/acs.inorgchem.9b01611
Inorg. Chem. XXXX, XXX, XXX−XXX

multiple cycles, as well as an easily regenerable form of sorbent. The calculations on the Zr-acetate model system clearly indicated different pK_a values for the bridging μ_3-OH groups, in agreement with the experimental pH titration results. These findings shed some light on the origin of high stability of UiO-66-NH_2 at different pH values in aqueous solution. In addition, the MOF@SiO_2 form demonstrated appreciable high uptake of model organic dyes, both of cationic and anionic nature, where the MOF selective uptake of either sorbates was effectively controlled by the solution pH. A detailed pH dependence of the MOF adsorption behavior toward guest molecules strongly indicated facile tunability of the chemistry of the nanocages by controlling the protonation state of the Zr cluster and pendant amino groups decorating the MOF cages. It is also concluded that the UiO-66-NH_2 has exceptional water stability characteristics and tunable charge state, stemming from the unique cage and cluster chemistry. The presence of amphoteric Zr-coordinated bridging oxide/hydroxyls, as well as pendant amine/ammonium groups, plays well toward facilitating the material *par excellence* performance as microporous sorbents in water treatment applications.

EXPERIMENTAL METHODS

The Zr-acetate cluster was optimized at the DFT (Density Functional Theory) level using the 6-311G(2p,2d)[52] basis set and the B3LYP[53,54] functional within the Gaussian 16[55] software. The desolvation energies and the electrostatic interactions between the oxo-bridges and Zr, carboxylate groups, and the other oxo-bridges were obtained by solving the Poisson−Boltzmann equation using adaptive Poisson−Boltzmann Solver (APBS).[32] Then, the MCCE (Multi-Conformer Continuum Electrostatics) method[33] was applied to generate Boltzmann distributions for all possible microstates at different pH with parametrization of the OH as reported previously.[3] The free energy of deprotonation is then calculated according to the following equation:

$$\Delta G^{(OH-O)} = [(pH - pK_{a,sol})] + \Delta G_{solvation} + \Delta G_{pairwise}$$

where $\Delta G^{(OH-O)}$ is the energy required to deprotonate the OH. $pK_{a,sol}$ is the solution pK_a of OH in water as obtained in Amin et al.[30] $\Delta\Delta G_{solvation}$ is the desolvation penalty, and $\Delta\Delta G_{pairwise}$ is the pair wise electrostatic interaction between OH and Zr, carboxylate groups, and the other oxo bridges.

Synthesis. ***Caution!*** *Concentrated HCl is highly corrosive and should be dealt with in a properly ventilated reaction fume hood while wearing proper protective equipment. Silica microparticles should be handled in a proper fumehood while wearing a proper protective mask to avoid inhalation.*

UiO-66-NH_2. In a clean scintillation vial, 2-aminoterephthalic acid (135.6 mg) was sonicated in 5 mL of DMF for 5 min to which was then added a separately prepared solution of $ZrCl_4$ (125.5 mg, in 5 mL of DMF, and 1 mL of HCl 37%). The vial was capped, and the mixture was left in an oven at 80 °C for 24 h. The solid was then filtered under a vacuum through a membrane filter and washed with ACN, then exchanged in ACN at 80 °C for 2 h and left in ACN at room temperature for 3 days. The solid was then filtered under a vacuum and dried in an oven at 80 °C for 2 h. Yield = 156.2 mg

UiO-66-NH_2@SiO_2. In a clean scintillation vial, a mixture of 2-aminoterephthalic acid (135.6 mg) and silica gel (224 mg) was mixed and sonicated in 5 mL of DMF for 5 min to which was then added a separately prepared solution of $ZrCl_4$ (125.5 mg, in 5 mL of DMF and 1 mL of HCl 37%). The vial was capped, and the mixture was stirred at 400 rpm for 2 h at 80 °C. The solid was then filtered under a vacuum through a membrane filter and washed with ACN, then exchanged in ACN at 80 °C for 2 h and left in ACN at room temperature for 24 h. The solid was then filtered under a vacuum and dried in an oven at 80 °C for 2 h. Yield = 346.6 mg (corresponding to 35.4 wt % MOF in the composite assuming a constant weight of silica).

Acid-Washing Procedure. In a clean scintillation vial, the desired amount of UiO-66-NH_2@SiO_2 was added to 10 mL of 0.1 M HCl and left for 10 min. The solid was then filtered under a vacuum through a nylon membrane filter, washed with 10 mL of Milli-Q deionized water (DI water), and dried in an isothermal oven at 80 °C for 45 min.

Calibration Curves for UV−vis Spectrophotometry. *Dichromate.* Different $K_2Cr_2O_7$ concentrations (2.5, 5, 10, 15, 20, and 25 ppm of Cr(VI)) were prepared. First, a solution of 100 ppm of Cr(VI) was prepared by dissolving 28.289 mg of $K_2Cr_2O_7$ in 100 mL of DI water, and subsequent dilutions were prepared with the desired concentrations. Finally, UV−vis spectrophotometry was used to get the absorbance of each of the prepared concentrations at λ_{max} 365 nm to construct the calibration curve. Three different calibration curves were prepared with various pH (5.4, 7.1, and 10.6).

Methyl Orange (MO). Different MO concentrations (2.5, 5, 10, 15, 20, and 25 ppm) were prepared. First, a solution of 100 ppm MO was prepared by dissolving 25 mg of MO in 250 mL of DI water, and subsequent dilutions were prepared with desired concentrations. Finally, UV−vis spectrophotometry was used to get the absorbance of each of the prepared concentrations at λ_{max} 464 nm to construct the calibration curve.

Methylene Blue (MB). Different MB concentrations (2.5, 5, 10, 15, 20, and 25 ppm) were prepared. First, a solution of 100 ppm MB was prepared by dissolving 25 mg of MB in 250 mL of DI water, and subsequent dilutions were prepared with desired concentrations. Finally, UV−vis spectrophotometry was used to get the absorbance of each of the prepared concentrations at λ_{max} 665 nm to construct the calibration curve.

Batch Adsorption Study. The reported weight of as-synthesized and acid-washed UiO-66-NH_2@SiO_2 utilized in dichromate or dyes uptake is the dry weight calculated based on observed weight loss from TGA measurement at 100 °C for each batch, as a moisture content of 7−18 wt % was observed in different batches depending on sample treatment and storage conditions.

Effect of Adsorbent Dose. *Methyl Orange.* Different weights of acid-washed UiO-66-NH_2@SiO_2 (13.2, 24.19, 49.77, and 74.29 mg) were added to four separate 10 mL MO samples (159 ppm) and stirred for 10 min. The suspension was then transferred to a 15 mL falcon tube and centrifuged at 6000 rpm for 10 min. One milliliter of the supernatant was then diluted five times prior to UV−vis spectrum acquisition.

Methylene Blue. Different weights of as-synthesized UiO-66-NH_2@SiO_2 (4.65, 9.3, 13.95, 18.6, and 23.25 mg) were added to four separate 10 mL MB samples (118 ppm) at pH 11.8 and stirred for 10 min. The suspension was then transferred to a plastic syringe and filtered through a PTFE syringe filter, which was previously washed with 5 mL of acetone and left to completely dry in air before usage. The filtrate was collected for UV−vis spectrum acquisition.

Effect of pH. *Dichromate.* Six separate stock solutions of 10 mL of 100 ppm dichromate were adjusted to the desired pH (2.7, 3.1, 5.2, 7.2, 10.3 and 11.4), to which 15 mg of acid-washed UiO-66-NH_2@SiO_2 was added separately to each vial. After stirring at 300 rpm for 10 min, the samples were centrifuged for 10 min at 6000 rpm and the supernatant was collected and diluted prior to UV−vis spectrum acquisition.

Methyl Orange. Six scintillation vials were prepared, each containing 10 mL of 160 ppm MO stock solution and 13.8 mg of the acid-washed UiO-66-NH_2@SiO_2, and the pH adjusted to desired pH (3.55, 4.63, 5.82, 6.73, 7.5 and 8.17) through the addition of HCl or NaOH solution. After stirring at 300 rpm for 10 min, the suspension was then filtered through a Nylon syringe filter, and 1 mL of the supernatant was collected and diluted five times prior to UV−vis spectrum acquisition.

Methylene Blue. Seven separate MB stock solutions of 10 mL of 121 ppm were prepared, and 13.95 mg of the as-synthesized UiO-66-NH_2@SiO_2 was added to each vial, then the pH adjusted to desired pH (3.46, 4.4, 5.08, 6.57, 7.38, 7.85, and 8.25) through the addition of

DOI: 10.1021/acs.inorgchem.9b01611
Inorg. Chem. XXXX, XXX, XXX−XXX

HCl or NaOH solution. After stirring at 300 rpm for 10 min, the suspension was transferred into a plastic syringe and filtered through a Nylon syringe filter. The filtrate was collected and diluted prior to UV−vis spectrum acquisition.

Adsorption Isotherm Studies. *Dichromate.* In sealed glass vials, seven separate samples of 41.2 mg of acid-washed UiO-66-NH_2@SiO_2 was added into 10 mL of Cr(VI) solutions of different concentrations (50, 100, 200, 400, 600, 800, and 1000 ppm) and stirred for 10 min. The suspensions were then centrifuged for 10 min at 6000 rpm, and the supernatant was collected and diluted prior to UV−vis spectrum acquisition.

Methyl Orange. In sealed glass vials, eight separate samples of 24.6 mg of acid-washed UiO-66-NH_2@SiO_2 was added into 10 mL of MO solutions of different concentrations (118, 159, 276, 385, 611, 833, 1019, 1222 ppm) and stirred for 10 min (pH 3.5). The suspensions were then centrifuged for 10 min at 6000 rpm, and 1 mL of the supernatant was collected and diluted prior to UV−vis spectrum acquisition. A control sample having 16 mg of silica and 10 mL of MO sample (1222 ppm) was conducted to calculate the actual adsorption capacity of the MOF.

Methylene Blue. In sealed glass vials, eight separate samples of 18.6 mg of as-synthesized UiO-66-NH_2@SiO_2 were added into 10 mL of MB solutions of different concentrations (118, 244, 522, 791, 1041, 1246, 1549, 1728 ppm) and stirred for 10 min (pH 9.5). The suspension was then transferred into a plastic syringe and filtered through a PTFE syringe filter, which was previously washed with 5 mL of acetone and left to completely dry in the air before usage. The filtrate was collected and diluted prior to UV−vis spectrum acquisition. A control sample having 11.5 mg of silica and 10 mL of MB sample (1549 ppm) was conducted to calculate the actual adsorption capacity of the MOF.

MOF Powder Adsorption Capacity for MB. A total of 18.6 mg of UiO-66-NH_2 was added into 10 mL of MB (2501 ppm, pH 9.5) and stirred for 10 min. The suspension was then transferred into a plastic syringe and filtered through a Nylon syringe filter. The filtrate was collected and diluted prior to UV−vis spectrum acquisition.

(Adsorption capacity = 1202 mg/g)

MOF Powder Adsorption Capacity for MO. A total of 23.25 mg of UiO-66-NH_2 was washed with 0.1 M HCl then added into 10 mL of MO (2127 ppm, pH 3.5) and stirred for 10 min. The suspension was then transferred into a plastic syringe and filtered through a Nylon string filter. The filtrate was collected and diluted prior to UV−vis spectrum acquisition.

(Adsorption capacity = 859 mg/g)

Zeta Potential Study. Separate samples of 10 mL of DI water were adjusted to the initial desired pH (2.7, 3.1, 5.2, 7.2, 10.3 and 11.4), then 1 mg of UiO-66-NH_2 was added to each sample, sonicated for 5 min, and let to equilibrate for 25 min before recording the final pH and measuring the zeta potential.

Potentiometric Titration. A total of 50 mg of UiO-66-NH_2 was added to 60 mL of 0.01 M sodium nitrate solution, sonicated briefly to fully disperse MOF particles, and left to soak for 18 h. The pH was the adjusted to 3 using 0.1 M HCl, and the suspension was then titrated with 0.1 M NaOH with an injection volume of 0.025 mL at a rate of 0.025 mL/min.

Regeneration Study. *Dichromate.* To probe the regeneration ability of UiO-66-NH_2@SiO_2, a 0.22 μm nylon syringe filter was loaded with 41.2 mg of acid-washed UiO-66-NH_2@ SiO_2 after being suspended in 10 mL of DI water. Then, 10 mL of 107 ppm of Cr(VI) solution was passed through the loaded syringe filter, and the filtrate was collected for UV−vis spectrum acquisition. The syringe filter was then washed with 1 M HCl followed by 10 mL of DI water. The dichromate uptake and washing were repeated for 10 cycles.

Methyl Orange. A PTFE syringe filter, which was previously washed with 5 mL of acetone, was loaded with 50 mg of acid-washed UiO-66-NH_2@SiO_2 after being suspended in 10 mL of DI water. Then, 5 mL of 119 ppm MO solution was passed through a loaded syringe filter, and the filtrate was collected for UV−vis spectrum acquisition. The syringe filter was then washed with 1 M HCl and acetone followed by DI water. The MO uptake and washing were repeated for 10 cycles.

Methylene Blue. A PTFE syringe filter, which was previously washed with 5 mL of acetone, was loaded with 50 mg of as-synthesized UiO-66-NH_2@SiO_2 after being suspended in 10 mL of DI water. Then, 5 mL of 94 ppm MB solution at pH 11.8 was passed through a loaded syringe filter, and the filtrate was collected for UV−vis spectrum acquisition. The syringe filter was then washed with 1 M NaOH (10 mL) followed by DI water (10 mL). The MB uptake and washing were repeated for 10 cycles.

■ ASSOCIATED CONTENT

Supporting Information

The Supporting Information is available free of charge on the ACS Publications website at DOI: 10.1021/acs.inorgchem.9b01611.

Further experimental details, FTIR spectra, gas sorption measurements, and further solution sorption characterization (PDF)

■ AUTHOR INFORMATION

Corresponding Author

*E-mail: malkordi@zewailcity.edu.eg.

ORCID

Stavros G. Karakalos: 0000-0002-3428-5433

Mohamed H. Alkordi: 0000-0003-1807-748X

Author Contributions

‖These authors contributed equally.

Notes

The authors declare no competing financial interest.

■ ACKNOWLEDGMENTS

The authors acknowledge Zewail City of Science and Technology for financial support (CMS-MA) and the support for the computational study by the U.S. Department of Energy, Office of Science, Office of Basic Energy Sciences, Division of Chemical Sciences, Geosciences, and Biosciences via grant DESC0001423 (M.R.G. and V.S.B.) and Dr. Marilyn Gunner for useful discussion.

■ REFERENCES

(1) Yaghi, O. M.; O'Keeffe, M.; Ockwig, N. W.; Chae, H. K.; Eddaoudi, M.; Kim, J. Reticular synthesis and the design of new materials. *Nature* **2003**, *423*, 705−714.

(2) Eddaoudi, M.; Moler, D. B.; Li, H.; Chen, B.; Reineke, T. M.; O'Keeffe, M.; Yaghi, O. M. Modular Chemistry: Secondary Building Units as a Basis for the Design of Highly Porous and Robust Metal−Organic Carboxylate Frameworks. *Acc. Chem. Res.* **2001**, *34*, 319−330.

(3) Elsaidi, S. K.; Mohamed, M. H.; Wojtas, L.; Chanthapally, A.; Pham, T.; Space, B.; Vittal, J. J.; Zaworotko, M. J. Putting the Squeeze on CH4 and CO2 through Control over Interpenetration in Diamondoid Nets. *J. Am. Chem. Soc.* **2014**, *136*, 5072−5077.

(4) Zhao, X.; Bu, X.; Zhai, Q. G.; Tran, H.; Feng, P. Pore space partition by symmetry-matching regulated ligand insertion and dramatic tuning on carbon dioxide uptake. *J. Am. Chem. Soc.* **2015**, *137*, 1396−1399.

(5) Plonka, A. M.; Banerjee, D.; Woerner, W. R.; Zhang, Z.; Nijem, N.; Chabal, Y. J.; Li, J.; Parise, J. B. Mechanism of carbon dioxide adsorption in a highly selective coordination network supported by direct structural evidence. *Angew. Chem., Int. Ed.* **2013**, *52*, 1692−1695.

(6) Huang, J. Q.; Zhuang, T. Z.; Zhang, Q.; Peng, H. J.; Chen, C. M.; Wei, F. Permselective graphene oxide membrane for highly stable

DOI: 10.1021/acs.inorgchem.9b01611
Inorg. Chem. XXXX, XXX, XXX−XXX

and anti-self-discharge lithium-sulfur batteries. *ACS Nano* **2015**, *9*, 3002−3011.
(7) Hu, T. L.; Wang, H.; Li, B.; Krishna, R.; Wu, H.; Zhou, W.; Zhao, Y.; Han, Y.; Wang, X.; Zhu, W.; Yao, Z.; Xiang, S.; Chen, B. Microporous metal-organic framework with dual functionalities for highly efficient removal of acetylene from ethylene/acetylene mixtures. *Nat. Commun.* **2015**, *6*, 7328.
(8) Falkowski, J. M.; Sawano, T.; Zhang, T.; Tsun, G.; Chen, Y.; Lockard, J. V.; Lin, W. Privileged phosphine-based metal-organic frameworks for broad-scope asymmetric catalysis. *J. Am. Chem. Soc.* **2014**, *136*, 5213−5216.
(9) McGuirk, C. M.; Katz, M. J.; Stern, C. L.; Sarjeant, A. A.; Hupp, J. T.; Farha, O. K.; Mirkin, C. A. Turning On Catalysis: Incorporation of a Hydrogen-Bond-Donating Squaramide Moiety into a Zr Metal-Organic Framework. *J. Am. Chem. Soc.* **2015**, *137*, 919−925.
(10) Zhu, Q. L.; Xu, Q. Metal-organic framework composites. *Chem. Soc. Rev.* **2014**, *43*, 5468−5512.
(11) Zhuang, X.; Gehrig, D.; Forler, N.; Liang, H.; Wagner, M.; Hansen, M. R.; Laquai, F.; Zhang, F.; Feng, X. Conjugated microporous polymers with dimensionality-controlled heterostructures for green energy devices. *Adv. Mater.* **2015**, *27*, 3789−3796.
(12) Katz, M. J.; Mondloch, J. E.; Totten, R. K.; Park, J. K.; Nguyen, S. T.; Farha, O. K.; Hupp, J. T. Simple and compelling biomimetic metal-organic framework catalyst for the degradation of nerve agent simulants. *Angew. Chem., Int. Ed.* **2014**, *53*, 497−501.
(13) Chaikittisilp, W.; Torad, N. L.; Li, C.; Imura, M.; Suzuki, N.; Ishihara, S.; Ariga, K.; Yamauchi, Y. Synthesis of nanoporous carbon-cobalt-oxide hybrid electrocatalysts by thermal conversion of metal-organic frameworks. *Chem. - Eur. J.* **2014**, *20*, 4217−4221.
(14) Hu, M.; Reboul, J.; Furukawa, S.; Radhakrishnan, L.; Zhang, Y.; Srinivasu, P.; Iwai, H.; Wang, H.; Nemoto, Y.; Suzuki, N.; Kitagawa, S.; Yamauchi, Y. Direct synthesis of nanoporous carbon nitride fibers using Al-based porous coordination polymers (Al-PCPs). *Chem. Commun. (Cambridge, U. K.)* **2011**, *47*, 8124−8126.
(15) Tang, J.; Yamauchi, Y. Carbon materials: MOF morphologies in control. *Nat. Chem.* **2016**, *8*, 638−639.
(16) Zhang, W.; Jiang, X.; Zhao, Y.; Carne-Sanchez, A.; Malgras, V.; Kim, J.; Kim, J. H.; Wang, S.; Liu, J.; Jiang, J. S.; Yamauchi, Y.; Hu, M. Hollow carbon nanobubbles: monocrystalline MOF nanobubbles and their pyrolysis. *Chemical science* **2017**, *8*, 3538−3546.
(17) Young, C.; Wang, J.; Kim, J.; Sugahara, Y.; Henzie, J.; Yamauchi, Y. Controlled Chemical Vapor Deposition for Synthesis of Nanowire Arrays of Metal-Organic Frameworks and Their Thermal Conversion to Carbon/Metal Oxide Hybrid Materials. *Chem. Mater.* **2018**, *30*, 3379−3386.
(18) Kandiah, M.; Nilsen, M. H.; Usseglio, S.; Jakobsen, S.; Olsbye, U.; Tilset, M.; Larabi, C.; Quadrelli, E. A.; Bonino, F.; Lillerud, K. P. Synthesis and Stability of Tagged UiO-66 Zr-MOFs. *Chem. Mater.* **2010**, *22*, 6632−6640.
(19) Guillerm, V.; Ragon, F.; Dan-Hardi, M.; Devic, T.; Vishnuvarthan, M.; Campo, B.; Vimont, A.; Clet, G.; Yang, Q.; Maurin, G.; Ferey, G.; Vittadini, A.; Gross, S.; Serre, C. A series of isoreticular, highly stable, porous zirconium oxide based metal-organic frameworks. *Angew. Chem., Int. Ed.* **2012**, *51*, 9267−9271.
(20) Furukawa, H.; Gandara, F.; Zhang, Y. B.; Jiang, J.; Queen, W. L.; Hudson, M. R.; Yaghi, O. M. Water adsorption in porous metal-organic frameworks and related materials. *J. Am. Chem. Soc.* **2014**, *136*, 4369−4381.
(21) Fei, H.; Shin, J.; Meng, Y. S.; Adelhardt, M.; Sutter, J. r.; Meyer, K.; Cohen, S. M. Reusable oxidation catalysis using metal-monocatecholato species in a robust metal−organic framework. *J. Am. Chem. Soc.* **2014**, *136*, 4965−4973.
(22) Siu, P. W.; Brown, Z. J.; Farha, O. K.; Hupp, J. T.; Scheidt, K. A. A mixed dicarboxylate strut approach to enhancing catalytic activity of a de novo urea derivative of metal-organic framework UiO-67. *Chem. Commun. (Cambridge, U. K.)* **2013**, *49*, 10920−10922.
(23) Rapti, S.; Pournara, A.; Sarma, D.; Papadas, I. T.; Armatas, G. S.; Hassan, Y. S.; Alkordi, M. H.; Kanatzidis, M. G.; Manos, M. J. Rapid, green and inexpensive synthesis of high quality UiO-66 amino-functionalized materials with exceptional capability for removal of hexavalent chromium from industrial waste. *Inorg. Chem. Front.* **2016**, *3*, 635−644.
(24) Li, X.; Xu, H.; Kong, F.; Wang, R. A Cationic Metal−Organic Framework Consisting of Nanoscale Cages: Capture, Separation, and Luminescent Probing of Cr2O72− through a Single-Crystal to Single-Crystal Process. *Angew. Chem., Int. Ed.* **2013**, *52*, 13769−13773.
(25) Fu, H.-R.; Xu, Z.-X.; Zhang, J. Water-stable metal−organic frameworks for fast and high dichromate trapping via single-crystal-to-single-crystal ion exchange. *Chem. Mater.* **2015**, *27*, 205−210.
(26) Shi, P. F.; Zhao, B.; Xiong, G.; Hou, Y. L.; Cheng, P. Fast capture and separation of, and luminescent probe for, pollutant chromate using a multi-functional cationic heterometal-organic framework. *Chem. Commun.* **2012**, *48*, 8231−8233.
(27) Zhang, Q.; Yu, J.; Cai, J.; Zhang, L.; Cui, Y.; Yang, Y.; Chen, B.; Qian, G. A porous Zr-cluster-based cationic metal−organic framework for highly efficient Cr 2 O 7 2− removal from water. *Chem. Commun.* **2015**, *51*, 14732−14734.
(28) Katz, M. J.; Brown, Z. J.; Colón, Y. J.; Siu, P. W.; Scheidt, K. A.; Snurr, R. Q.; Hupp, J. T.; Farha, O. K. A facile synthesis of UiO-66, UiO-67 and their derivatives. *Chem. Commun.* **2013**, *49*, 9449.
(29) Vermoortele, F.; Bueken, B.; Le Bars, G.; Van de Voorde, B.; Vandichel, M.; Houthoofd, K.; Vimont, A.; Daturi, M.; Waroquier, M.; Van Speybroeck, V.; Kirschhock, C.; De Vos, D. E. Synthesis modulation as a tool to increase the catalytic activity of metal-organic frameworks: the unique case of UiO-66(Zr). *J. Am. Chem. Soc.* **2013**, *135*, 11465−11468.
(30) Graf, N.; Yegen, E.; Gross, T.; Lippitz, A.; Weigel, W.; Krakert, S.; Terfort, A.; Unger, W. E. S. XPS and NEXAFS studies of aliphatic and aromatic amine species on functionalized surfaces. *Surf. Sci.* **2009**, *603*, 2849−2860.
(31) Wang, Y.; Li, L. J.; Dai, P. C.; Yan, L. T.; Cao, L.; Gu, X.; Zhao, X. B. Missing-node directed synthesis of hierarchical pores on a zirconium metal-organic framework with tunable porosity and enhanced surface acidity via a microdroplet flow reaction. *J. Mater. Chem. A* **2017**, *5*, 22372−22379.
(32) Allen, G. C.; Tucker, P. M. Multiplet splitting of X-ray photoelectron lines of chromium complexes. The effect of covalency on the 2p core level spin-orbit separation. *Inorg. Chim. Acta* **1976**, *16*, 41−45.
(33) Harrison, P. G.; Lloyd, N. C.; Daniell, W. The Nature of the Chromium Species Formed during the Thermal Activation of Chromium-Promoted Tin(IV) Oxide Catalysts: An EPR and XPS Study. *J. Phys. Chem. B* **1998**, *102*, 10672−10679.
(34) Aguilera-Sigalat, J.; Bradshaw, D. A colloidal water-stable MOF as a broad-range fluorescent pH sensor via post-synthetic modification. *Chem. Commun. (Cambridge, U. K.)* **2014**, *50*, 4711−4713.
(35) Haque, E.; Jun, J. W.; Jhung, S. H. Adsorptive removal of methyl orange and methylene blue from aqueous solution with a metal-organic framework material, iron terephthalate (MOF-235). *J. Hazard. Mater.* **2011**, *185*, 507−511.
(36) Wu, S. C.; You, X.; Yang, C.; Cheng, J. H. Adsorption behavior of methyl orange onto an aluminum-based metal organic framework, MIL-68(Al). *Water Sci. Technol.* **2017**, *75*, 2800−2810.
(37) Salama, R. S.; El-Hakama, S. A.; Samraa, S. E.; El-Dafrawya, S. M.; Ahmeda, A. I. Adsorption, Equilibrium and Kinetic Studies on the Removal of Methyl Orange Dye from Aqueous Solution by Using of Copper Metal Organic Framework (Cu-BDC). *Int. J. Modern Chem.* **2018**, *10*, 195−207.
(38) GONG, W. Adsorption of Methylene Blue by Phosphomolybdiumtungstic Acid Decorated Metal Organic Framework MOF-5. *Chinese Journal of Applied Chemistry* **2016**, *33*, 1047−1055.
(39) Zhao, S. Q.; Chen, D.; Wei, F. H.; Chen, N. N.; Liang, Z.; Luo, Y. Synthesis of graphene oxide/metal-organic frameworks hybrid materials for enhanced removal of Methylene blue in acidic and alkaline solutions. *J. Chem. Technol. Biotechnol.* **2018**, *93*, 698−709.
(40) Zhou, Y.; Qin, L.; Wu, M. K.; Han, L. A Bifunctional Anionic Metal-Organic Framework: Reversible Photochromism and Selective

DOI: 10.1021/acs.inorgchem.9b01611
Inorg. Chem. XXXX, XXX, XXX−XXX

Adsorption of Methylene Blue. *Cryst. Growth Des.* **2018**, *18*, 5738−5744.
(41) Karimi, M. A.; Masrouri, H.; Mirbagheri, M. A.; Andishgar, S.; Pourshamsi, T. Synthesis of a new magnetic metal−organic framework nanocomposite and its application in methylene blue removal from aqueous solution. *J. Chin. Chem. Soc.* **2018**, *65*, 1229−1238.
(42) Huang, L.; Cai, J.; He, M.; Chen, B.; Hu, B. Room-Temperature Synthesis of Magnetic Metal−Organic Frameworks Composites in Water for Efficient Removal of Methylene Blue and As (V). *Ind. Eng. Chem. Res.* **2018**, *57*, 6201−6209.
(43) Bibi, R.; Wei, L.; Shen, Q.; Tian, W.; Oderinde, O.; Li, N.; Zhou, J. Effect of amino functionality on the uptake of cationic dye by titanium-based metal organic frameworks. *J. Chem. Eng. Data* **2017**, *62*, 1615−1622.
(44) Mohammadi, A. A.; Alinejad, A.; Kamarehie, B.; Javan, S.; Ghaderpoury, A.; Ahmadpour, M.; Ghaderpoori, M. Metal-organic framework Uio-66 for adsorption of methylene blue dye from aqueous solutions. *Int. J. Environ. Sci. Technol.* **2017**, *14*, 1959−1968.
(45) Azhar, M. R.; Abid, H. R.; Sun, H.; Periasamy, V.; Tadé, M. O.; Wang, S. One-pot synthesis of binary metal organic frameworks (HKUST-1 and UiO-66) for enhanced adsorptive removal of water contaminants. *J. Colloid Interface Sci.* **2017**, *490*, 685−694.
(46) Qiu, J.; Feng, Y.; Zhang, X.; Jia, M.; Yao, J. Acid-promoted synthesis of UiO-66 for highly selective adsorption of anionic dyes: Adsorption performance and mechanisms. *J. Colloid Interface Sci.* **2017**, *499*, 151−158.
(47) Chen, Q.; He, Q.; Lv, M.; Xu, Y.; Yang, H.; Liu, X.; Wei, F. Selective adsorption of cationic dyes by UiO-66-NH2. *Appl. Surf. Sci.* **2015**, *327*, 77−85.
(48) Morris, W.; Wang, S.; Cho, D.; Auyeung, E.; Li, P.; Farha, O. K.; Mirkin, C. A. Role of Modulators in Controlling the Colloidal Stability and Polydispersity of the UiO-66 Metal-Organic Framework. *ACS Appl. Mater. Interfaces* **2017**, *9*, 33413−33418.
(49) Klet, R. C.; Liu, Y.; Wang, T. C.; Hupp, J. T.; Farha, O. K. Evaluation of Brønsted acidity and proton topology in Zr- and Hf-based metal−organic frameworks using potentiometric acid−base titration. *J. Mater. Chem. A* **2016**, *4*, 1479−1485.
(50) Chin, J. M.; Chen, E. Y.; Menon, A. G.; Tan, H. Y.; Hor, A. T. S.; Schreyer, M. K.; Xu, J. Tuning the aspect ratio of NH2-MIL-53(Al) microneedles and nanorods via coordination modulation. *CrystEngComm* **2013**, *15*, 654−657.
(51) Trickett, C. A.; Gagnon, K. J.; Lee, S.; Gandara, F.; Burgi, H. B.; Yaghi, O. M. Definitive molecular level characterization of defects in UiO-66 crystals. *Angew. Chem., Int. Ed.* **2015**, *54*, 11162−11167.
(52) Krishnan, R.; Binkley, J. S.; Seeger, R.; Pople, J. A. Self-consistent molecular orbital methods. XX. A basis set for correlated wave functions. *J. Chem. Phys.* **1980**, *72*, 650−654.
(53) Becke, A. D. Density-functional thermochemistry. III. The role of exact exchange. *J. Chem. Phys.* **1993**, *98*, 5648−5652.
(54) Lee, C.; Yang, W.; Parr, R. G. Development of the Colle-Salvetti correlation-energy formula into a functional of the electron density. *Phys. Rev. B: Condens. Matter Mater. Phys.* **1988**, *37*, 785−789.
(55) Frisch, M. J.; Trucks, G. W.; Schlegel, H. B.; Scuseria, G. E.; Robb, M. A.; Cheeseman, J. R.; Scalmani, G.; Barone, V.; Petersson, G. A.; Nakatsuji, H.; Li, X.; Caricato, M.; Marenich, A. V.; Bloino, J.; Janesko, B. G.; Gomperts, R.; Mennucci, B.; Hratchian, H. P.; Ortiz, J. V.; Izmaylov, A. F.; Sonnenberg, J. L.; Williams-Young, D.; Ding, F.; Lipparini, F.; Egidi, F.; Goings, J.; Peng, B.; Petrone, A.; Henderson, T.; Ranasinghe, D.; Zakrzewski, V. G.; Gao, J.; Rega, N.; Zheng, G.; Liang, W.; Hada, M.; Ehara, M.; Toyota, K.; Fukuda, R.; Hasegawa, J.; Ishida, M.; Nakajima, T.; Honda, Y.; Kitao, O.; Nakai, H.; Vreven, T.; Throssell, K.; Montgomery, J. A., Jr.; Peralta, J. E.; Ogliaro, F.; Bearpark, M. J.; Heyd, J. J.; Brothers, E. N.; Kudin, K. N.; Staroverov, V. N.; Keith, T. A.; Kobayashi, R.; Normand, J.; Raghavachari, K.; Rendell, A. P.; Burant, J. C.; Iyengar, S. S.; Tomasi, J.; Cossi, M.; Millam, J. M.; Klene, M.; Adamo, C.; Cammi, R.; Ochterski, J. W.; Martin, R. L.; Morokuma, K.; Farkas, O.; Foresman, J. B.; Fox, D. J. *Gaussian 16*, version B.01; Gaussian, Inc.: Wallingford, CT, 2016.

DOI: 10.1021/acs.inorgchem.9b01611
Inorg. Chem. XXXX, XXX, XXX−XXX